2023

Enhancing the Thermo-Optic Tuning Performance of Whispering Gallery Modes in a Microcapillary Resonator Filled With Nematic Liquid Crystals

Zhe Wang
Technological University Du, Zhe.Wang@mytudublin.ie

Arun Kumar Mallik
Tyndall National Institute, University College Dublin, Ireland

fangfang Wei
Technological University Dublin, fangfang.wei@tudublin.ie

See next page for additional authors

Funder: This research was funded by the TU Dublin Fiosraigh Scholarship Award 2019

Enhancing the thermo-optic tuning performance of whispering gallery modes in a microcapillary resonator filled with nematic liquid crystals

Zhe Wang[a,*], Arun Kumar Mallik[b], Fangfang Wei[a], Zhuochen Wang[a], Anuradha Rout[a], Qiang Wu[c], Yuliya Semenova[a]

a Photonics Research Centre, School of Electrical and Electronic Engineering, Technological University Dublin, Dublin Ireland.
b Tyndall National Institute, University College Cork, Lee Maltings, Dyke Parade, Cork, Ireland.
c Department of Mathematics, Physics and Electrical Engineering, Northumbria University, Newcastle Upon Tyne NE1 8ST, UK.

* D19125415@mytudublin.ie

Abstract:

We investigated both theoretically and experimentally, the thermo-optic tuning of whispering-gallery modes (WGMs) in a microcapillary resonator filled with nematic liquid-crystal (LCs). The tuning of WGMs was realized due to the photo-thermal effect of magnetic nanoparticles (MNPs) on the surface of a fiber half-taper connected to a pump laser source, resulting in temperature-induced refractive index (RI) changes of the LC material. Based on perturbation theory, we analyzed the influence the RI and the wall thickness on the sensitivity of the proposed tuning scheme. Furthermore, we experimentally demonstrated that increasing the thickness of the MNPs coating on the fiber taper surface leads to a stronger photo-thermal effect and to a larger RI change of the LC material within the microcapillary core. Thermo-optic tuning of WGM resonances with a sensitivity of 256.63±5.67 pm/mW to the laser pump power and tuning range of 10.43 nm has been achieved. The developed thermo-optic tuning scheme has many potential applications as tunable devices, optical filters and sensors.

Keywords: Whispering gallery modes (WGMs), Liquid crystals (LCs), Capillary, Thermo-optic tuning, Refractive index (RI)

1.Introduction

Whispering gallery mode (WGM) resonators have attracted significant interest for various applications in nonlinear optics[1], microcavity lasers[2], optical signal processing[3], and optical sensing[4] due to their small mode volumes and high Q factors. A typical WGM resonator setup consists of a circular dielectric resonator structure with a higher refractive index (RI) than its surrounding medium and a tapered fiber or a prism for coupling of light into the resonator[5]. A wide variety of resonator geometries that support WGMs have been proposed to date, such as microspheres[6], microcapillaries[7], microcylinders[8], microrings[9], and microbottles[10]. The microcapillary based resonators have become especially popular in sensing due to their simple fabrication and ease of integration with microfluidic platforms. Such a microcapillary resonator can act both as a sensing element and a fluid channel, where the analyte interacts with the electromagnetic field near the microcapillary walls. Moreover, due to their sensitivity, a very low

concentration of molecules can be detected using microcapillary based WGM, such as for example, proteins[11] and nucleic acids[12], which is important in many biosensing applications.

Among the variety of studies of microcapillary-based WGM resonators, photothermal tuning of their properties has become a topic of special interest due to its high efficiency (high temperature sensitivity) and a relatively short response time in comparison with other tuning methods. Due to the excellent light-to-heat conversion properties of Fe_3O_4 magnetic nanoparticles (MNPs) within magnetic fluids[13], several photothermal tuning schemes have been proposed recently, for example, by directly focusing an external laser spot on the capillary infiltrated with a magnetic fluid[14] or by splicing the fiber with a magnetic-fluid-infiltrated microstructured optical fiber[15]. MNPs are heated under the influence of pump laser radiation, which results in the change of the effective RI and the effective radius due to the thermos-optic and thermal expansion effects respectively, consequently leading to WGM resonant wavelengths tuning. However, poor uniformity of the magnetic fluids in the above-mentioned tunable resonators is inevitable due to sedimentation of MNPs with time in the capillary or fiber cavity. In addition, immediate sealing off the microfiber containers is required to avoid the dry-out in water-based magnetic fluids.

On the other hand, LCs infiltrated photonic crystal fiber (PCF) or capillary has been studied for its application in tuning system and fiber laser system due to its properties of birefringence and high thermo- & electro-optic coefficients. On this basis, some tuning methods have been explored to develop cylindrical tuning system, such as thermal-optical and electronic-optical. Traditional thermal tuning usually relies on the extra heating source providing temperature control. However, the response time of these scheme are relatively longer giving the gap distance between heater source and cylindrical resnoator structure[16]. There are also reports on the exploration of electrically tuned PCFresonator, but these schemes usually need extra electrical field trigged by parallel electrodes in close spots, which might be challenging for constructing fragile microresonator structures[17,18].

Recently we proposed and experimentally demonstrated a novel thermo-optic tuning scheme based on a microcapillary resonator filled with nematic liquid crystal (LCs), where WGMs tuning was realized by placing a fiber half-taper coated with a thin layer of MNPs connected to a pump laser source[19]. Due to the excellent light-to-heat conversion of MNPs, the increase of temperature of the nematic LC causes changes in the effective RI of the nematic LCs and the corresponding spectral shift of the WGM resonances. The proposed scheme allows to overcome the issues associated with sedimentation of MNPs and lack of stability of previously reported photothermally tuned WGM resonators.

In order to improve understanding of the proposed tuning mechanism and to optimize its performance, in this paper we for the first time theoretically analyzed the influence of the core RI and the capillary wall thickness on the tuning sensitivity and tuning range. Based on the results of the analysis, we further investigated the proposed tuning scheme experimentally and demonstrated that an enhanced sensitivity to the pump laser power can be achieved by increasing the thickness of the MNPs coating on the fiber taper surface. In this work, a tuning sensitivity of 256.63±5.67 pm/mW and tuning range of 10.43 nm, which are 1.75 and 3.2 times higher than that in the previous report achieved. This work is the first comprehensive

study of the proposed tuning structure and can be useful for the design of tunable optical filters and sensors based on the proposed structure.

2.Materials and methods

A tapered fiber with a 10 μm uniform waist diameter was fabricated from a standard single-mode telecommunications fiber (SMF-28 from Corning) by using a custom-built microheater brushing setup[20]. In our experiment, a customized computer program controlled the stretching motion of the fiber within the microheater slit where the temperature was approximately 1300 °C. The full taper then was cut in the middle of its uniform waist section to create two half-tapers which were subsequently coated with MNPs (Micromod Partikeltechnologie GmbH, nanomag@-D, 09-20-132) by dipping into and pulling out from a solution of MNPs at a rate of 0.5 mm/s. The MNPs solution was adhered on the surface of the half-taper due to the surface tension. The coated half-tapers then were cured at room temperature for 48 hours. As a result, a thin coating layer of MNPs was applied over a short length of the half-taper adjacent to its end tip. The half-tapers with different coating thicknesses of MNPs layers were achieved by repeating the coating process and adjusting the concentration of the MNPs solution. Specifically, the coated half-taper was dipped in pulling out from a solution of MNPs using the same rate after being cured for 48 hours. Figs. 1(a)-(c) show scanning electron microscope (SEM) images of the MNPs layers on the surfaces of half-tapers subjected to different number of coating cycles. The thickness of MNPs increased from 99.2 nm to 340 nm with the increase of the number of coating cycles from 1 to 3, which demonstrates the increase of the number of MNPs on the surface of the half-taper. The energy dispersive X-ray (EDX) spectroscopy of the half-taper subjected to a single coating cycle is shown in Fig. 1(d). The presence of iron (Fe) in the spectrogram confirms successful deposition of the MNPs on the half-taper surface.

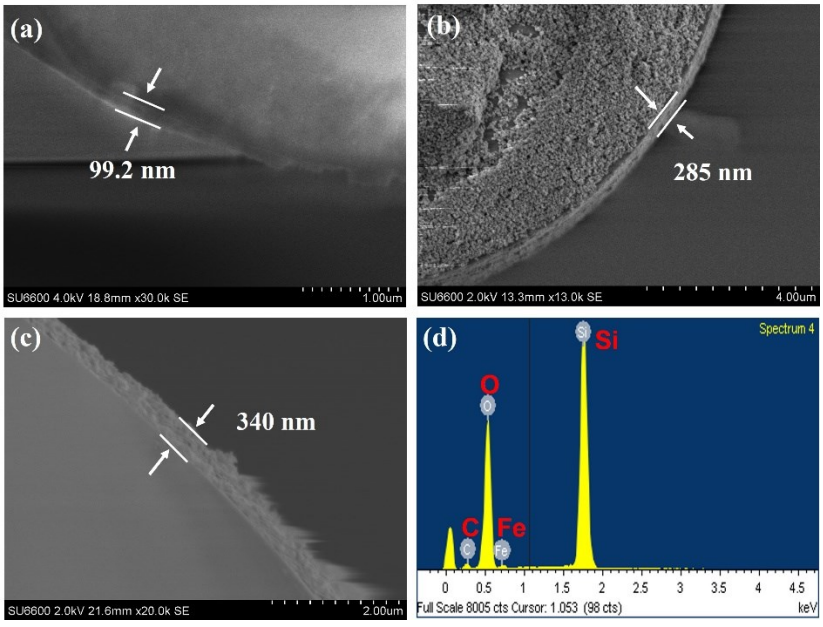

Fig. 1. SEM images of the fiber half-taper dip-coated with different thickness of MNPs layers: (a) a single cycle coating, (b) two coating cycles, (c) three coating cycles, (d) measured EDX spectroscopy of the coating area.

A thin-wall (1-2 μm) capillary with an external diameter of 45 μm was fabricated by heating and stretching a commercial silica capillary (Polymicro Technology) with the outer/inner diameters of 850 μm and 700 μm respectively. The fabricated capillary was then fixed on a glass slide using two drops of a UV curable epoxy to improve mechanical stability.

Another full fiber taper with a uniform waist diameter of 1 μm was then fabricated using the ceramic microheater setup. To realize light coupling into the capillary resonator, the resonator and the fiber taper were placed perpendicularly and in close proximity with each other using two different translation stages. A broadband light source (BBS) (Thorlabs, S5FC1005S(P), 1500–1600 nm, diode current = 600 mA, FWHM = 50 nm) connected to the input port of the tapered fiber through a polarization controller provided a stable light input, and an optical spectrum analyzer (OSA, Advantest, Q8384, resolution=0.01 nm) was used to monitor the WGM spectra of the capillary at the output of the tapered fiber. After adjusting the position of the fiber taper with respect to the capillary, the transmission spectrum with strong WGM dips was observed on the screen of the OSA. The extinction ratio of the WGM spectrum was further improved by adjusting the input light polarization by means of polarization controller. Finally, both ends of the fiber taper were fixed on a glass slide using a UV curable epoxy.

To fabricate the WGM capillary resonator, a kind of nematic LC, MDA-05-2782 (n_e=1.6152, n_o=1.4912, measured at 589.3 nm and 20 °C, clearing point-106°C) (Licristal, Merck) was firstly injected into the capillary at room temperature using a syringe from one of the capillary ends. Following the injection, the fiber half-taper coated with MNPs and the LC-infiltrated capillary were fixed on two separate micro-translation stages. By precisely controlling both translation stages, the fiber tip was inserted into the capillary and its tip position inside the capillary was adjusted close to the light coupling point. The half-taper was then fixed on the glass slide using a UV curable epoxy.

The schematic diagram of the experimental setup is shown in Fig. 2. One part of the experimental setup is similar to the traditional capillary resonator setup, which consists of a BBS, capillary resonator, a polarization controller, and an OSA. Meanwhile, the optical tuning was realized by connecting a 980 nm laser (Superlum, Pilot-6, 300 mW) to the free end of the MNPs coated half-taper. To precisely control tunning and maximize the tuning range, the 13.3% splitting power ratio end of an optical splitter was connected to an optical power meter (dBm Optics, Model 4100) whereas the 86.7% splitting power ratio end was connected to the MNPs coated half-taper.

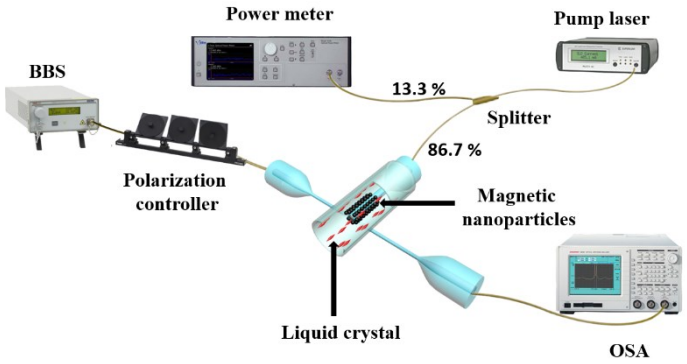

Fig. 2. Schematic diagram of the LC-infiltrated capillary WGM resonator and experimental setup for its characterization.

3. Theoretical analysis and simulations

In order to optimize the parameters of the proposed tuning scheme, it is useful to consider and analyze the changes in resonant wavelengths, and corresponding mode field distributions within the WGM capillary resonator under different conditions. For simplicity we consider only the fundamental TE modes, in accordance with TE filed equations for the cylindrical WGM resonator[21]:

$$E(r) = \begin{cases} A_l J_l(n_1 kr), & r \le b \\ B_l H_l^{(2)}(n_2 kr) & + H_l^{(1)}(n_2 kr), b < r \le a \\ D_l H_l^{(1)}(n_3 kr), & r > a \end{cases} \quad (1)$$

where r is the radial direction of the capillary, a and b are the outer and inner radii of the capillary, J_l is the cylindrical Bessel function of the first kind with angular mode number l, $H_l^{(1)}$ and $H_l^{(2)}$ are cylindrical Hankel functions with order l, k is the vacuum wavevector, A_l, B_l, and D_l are constants. In accordance with the continuity of electromagnetic filed at the dielectric interface, the resonant wavelength for the TE mode with the mode number l can be calculated as follows[21]:

$$\frac{n_3 H_l^{(1)\prime}(n_3 ka)}{n_2 H_l^{(1)}(n_3 ka)} = \frac{B_l H_l^{(2)\prime}(n_2 ka) + H_l^{(1)\prime}(n_2 ka)}{B_l H_l^{(2)}(n_2 ka) + H_l^{(1)}(n_2 ka)} \quad (2)$$

$$B_l = \frac{n_2 J_l(n_1 kb) H_l^{(1)\prime}(n_2 kb) - n_1 J_l'(n_1 kb) H_l^{(1)}(n_2 kb)}{-n_2 J_l(n_1 kb) H_l^{(2)\prime}(n_2 kb) + n_1 J_l'(n_1 kb) H_l^{(2)}(n_2 kb)} \quad (3)$$

where r is the radial direction of the capillary, a and b are the outer and inner radii of the capillary, J_l is the cylindrical Bessel function of the first kind with order l, $H_l^{(1)}$ and $H_l^{(2)}$ are cylindrical Hankel functions with order l, $H_l^{(1)\prime}$ and $H_l^{(2)\prime}$ are the derivatives of the cylindrical Hankel functions with order l, k is the vacuum wavevector, n_1, n_2, and n_3 are the RIs of the capillary core material, capillary wall and the surrounding air.

Using equations 2 and 3, the resonance wavelength with respect to different capillary wall thicknesses (1 µm, 1.5 µm, 2 µm, 2.5 µm) at different RIs (from 1.4 to 1.55) can be calculated as shown in Fig. 3(a) for the fundamental mode with l = 153 in a capillary with an outer radius a = 27.6 µm, n_2 = 1.44, n_3 = 1. As one can see from the graph, the resonance wavelength experiences red shift as the core material RI increases for all the simulated capillary wall thicknesses. A greater wavelength shift can be observed when the wall thickness decreases and the core RI increases. Meanwhile, an increasing sensitivity trend can be demonstrated for a specific case as the RI increases, especially when the RI of the capillary core material is greater than RI of the silica wall. When the RI of the capillary core material equals to the RI of silica wall (n_1=n_2=1.44), the resonance wavelengths for all the cases with different wall thicknesses are equal to each other, which means the nematic LCs infiltrated WGM can be seen as a solid silica cylinder. The RI sensitivity for the TE polarized mode (S_{TE}) can be calculated as:

$$S_{TE} = \frac{\lambda_0}{n_1} * \frac{I_1}{I_1+I_2+I_3} \qquad (4)$$

where I_1, I_2, and I_3 are the volume-integrated electric field intensities in the capillary core, capillary wall and the surrounding medium, respectively[21]. Fig. 3(b) illustrates the RI sensitivity as a function of RI for different capillary wall thicknesses. It can be seen that the RI sensitivity of the resonator increases with the increase of RI, which is consistent with the trend illustrated Fig. 3(a). It also shows that the RI sensitivity of the capillary resonator with thinner walls is greater than that of the capillary with thicker walls at the same RI value.

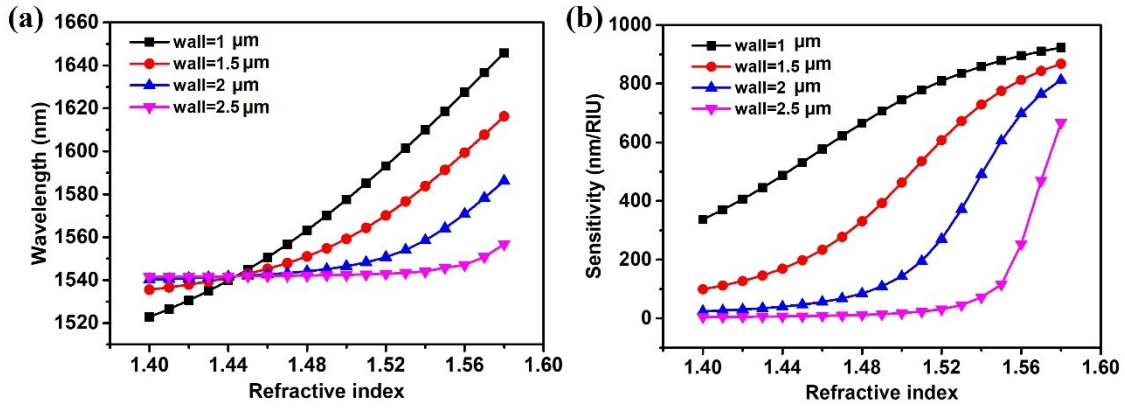

Fig. 3. (a) Resonance wavelength for the TE mode (l=153) as a function of core material RI for the capillaries with 1-μm, 1.5-μm, 2-μm, and 2.5-μm wall thickness, (b) calculated sensitivity versus core material RI for the capillaries with 1-μm, 1.5-μm, 2-μm, and 2.5-μm wall thickness.

The increasing sensitivity of capillary with the increase of RI can be explained by the increase of the proportion of mode field energy distributed in the capillary core. The electric field intensity $|\boldsymbol{E}(\boldsymbol{r})|^2$ distributions for the case of 1.5-µm wall thickness are shown in Fig. 4(a) for different core RIs. Fig. 4(b) illustrates changes in the fractions of the mode energy within the capillary core (f_1), capillary wall (f_2)

and the surrounding medium (f_3) with the increase of the core RI. As can be seen from the graphs, as the core RI increases, greater fraction of the mode energy moves from the capillary wall and surrounding inside the capillary core. To illustrate the changes in the mode distributions, Fig. 4(c) presents the electric filed distributions for liquid filled capillary with different RIs and mode order numbers using COMSOL Multiphysics (5.5). As can be seen from the graphs, the electric field maximum for the fundamental mode (1st order mode) is inside the capillary wall whereas the field maxima for the 2nd and 3rd order modes are located inside the capillary core. Similar trend is observed for all three modes with the increase of the core RI, which results in the mode energy moving away from the capillary wall inside the capillary core, which leads to a higher effective RI ($n_{eff} = f_1 n_1 + f_2 n_2 + f_3 n_3$) and higher RI sensitivity. Thus utilizing nematic LCs with a relatively high RI in our experiment allows to realize an efficient tuning of the WGM spectrum with high RI sensitivity. Moreover, the simulation shows that a thin-walled WGM cylindrical resonator should be used to increase the RI sensitivity in the tuning experiment.

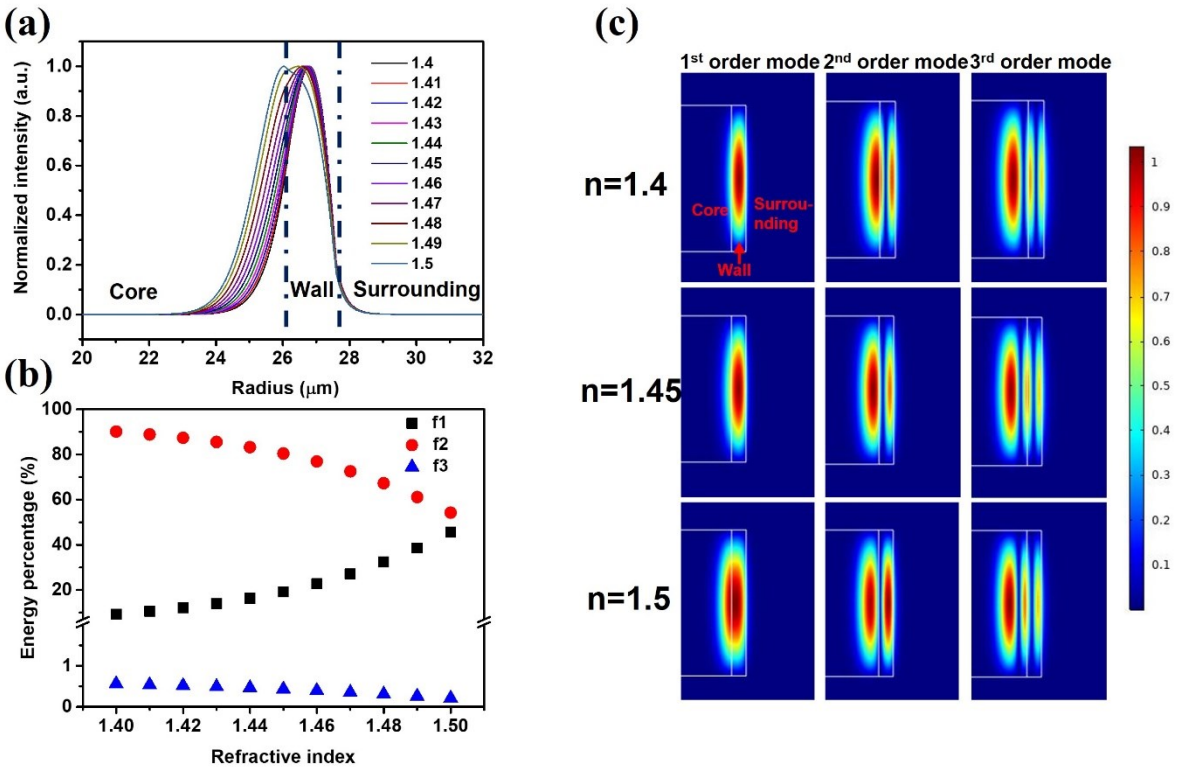

Fig. 4. (a) simulated TE-polarized electric field intensity $|E(r)|^2$ at different values of the capillary core RIs for the capillary with 1.5-μm wall thickness, (b) fractions of the mode energy in the capillary core (f_1), capillary wall (f_2) and the surrounding medium (f_3) corresponding to the RI values in Fig. 4(a), (c) simulated mode distributions for the capillary with different RI and order number settings.

4. Results and discussion

Fig. 5 shows a typical experimentally measured transmission spectrum for the WGM resonator infiltrated with MDA-05-2782 (MDA-WDM) after inserting the MNPs coated tapered fiber into the infiltrated capillary. The Q-factor of the MDA-WDM spectrum is calculated using the following equation:

$$Q = \frac{\lambda}{FWHM}$$

where λ represents the resonance wavelength and FWHM represents its full width at half maximum. The Q-factor of the selected resonance near 1518 nm was estimated as 6.08×10^3.

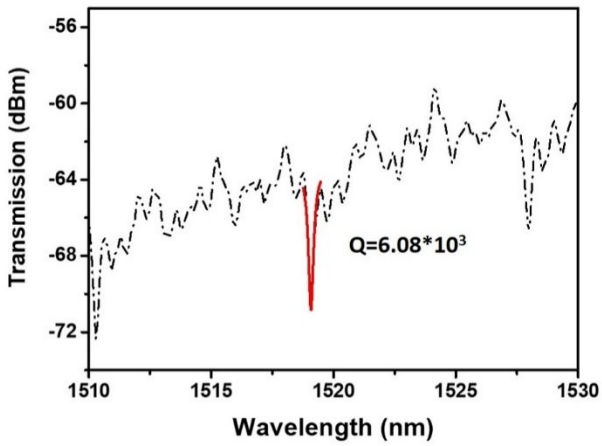

Fig. 5. Transmission spectrum of the MDA-WGM with a half taper (10 mg/ml MNPs concentration) coated with a single MNPs layer.

To study the optical tuning of the MDA-WGM, the transmission spectra at each state were recorded using a customized LabVIEW PC program-controlled OSA where the pump laser power launched into the MNPs coated half-taper increased from 0 to 36.4 mW with a step of 5.2 mW, and then decreased with the same step back to 0. This experiment was repeated for the MDA-WGM resonators with the fiber half-tapers having different thickness of the MNPs coating. To minimize the external temperature perturbations and reduce the errors, the setup was placed in a thermally- insulated chamber and the transmission spectra were collected 5 times at each pump power state.

Fig. 6(a) shows the experimentally measured transmission spectra of the MDA-WGM with a single coating cycle of the half-taper (10 mg/ml MNPs concentration) at different levels of the pump laser power. As can be seen from the graph, an increase in the pump laser power from 0 to 36.4 mW results in a blue shift of the MDA-WGM spectrum, while a decrease in the pump laser power leads to a red spectral shift and a gradual return back to its original position when the pump laser is turned off. Fig. 6(b) illustrates the dependence of the selected MDA-WGM resonant dip versus the pump laser power. The resonant dip at circa 1520 nm was selected to study the shift of the resonance wavelength. It was found that the resonant dips in

the WGM spectrum shift linearly with the applied pump laser power. The maximum tuning range for the MDA-WGM was 5.38 nm and the linear fitting dependencies were $y = -0.146x + 1519.86$ and $y = -0.1463x+1519.936$, with the sensitivity to pump power of 146.15±0.15 pm/mW. Fig. 6(c) summarizes the Q-factors of the selected dips in Fig. 6(b) versus the pump laser power. As can be seen from Fig. 6(c), the Q-factor fluctuates around 4667 and with a slight tendency to decrease with the pump laser power. This is consistent with the results of the previously reported study of the temperature dependence of Q factor in LC-droplet resonators[22], where it was found that an increase in temperature leads to a decrease in the orientational order within the LC droplets and the resonators' Q factor.

The tunability and sensitivity of the MDA-WGM based on the same structure with different thicknesses of the MNPs coating on the half-tapers' surface were investigated and the results are presented in Fig. 6(d). The measured tuning ranges for the selected dips around 1520-1530 nm for the MDA-WGM resonators with half tapers coated with a single layer of MNPs were: 1.26 nm for MNPs concentration of 2 mg/ml, 2.27 nm for MNPs concentration of 4 mg/ml, and 5.38 nm for MNPs concentration of 10 mg/ml. For the MDA-WGM resonators with the half-tapers subjected to 2 and 3 coating cycles with MNPs in concentration of 10 mg/ml, the corresponding tuning ranges were 7.8 nm and 10.43 nm, respectively. The corresponding sensitivities are 35±0.8 pm/mW, 66.9±2.5 pm/mW, 146.15±0.15 pm/mW, 238.93±3.2 pm/mW, and 256.63±5.67 pm/mW. The maximum tuning range and sensitivity were achieved in the case of the MDA-WGM with a half-taper subjected to 3-coating cycles with MNPs in concentration of 10 mg/ml. The higher sensitivity can be explained by a larger amount of MNPs on the surface of the half-taper leading to a greater radiation absorption and to a stronger photothermal effect.

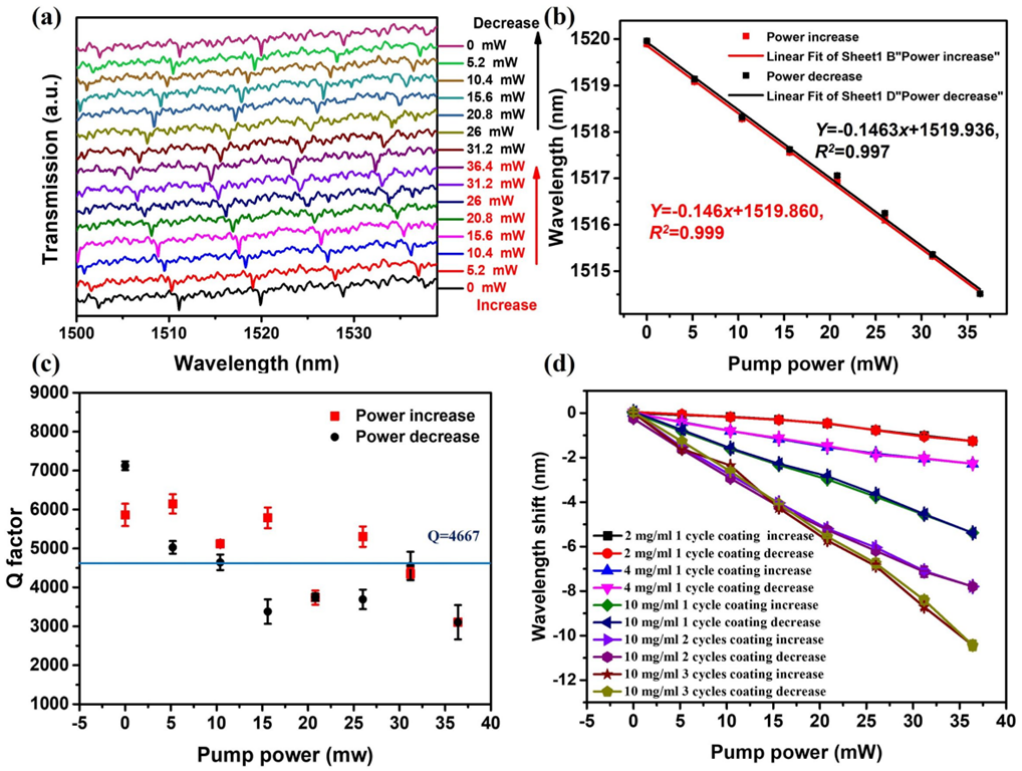

Fig. 6. (a) Transmission spectrum of the MDA-WGM with a single coating cycle of fiber half taper (10 mg/ml MNPs concentration) at different values of laser power launched into the capillary through the half-taper, (b) experimental data and linear fitting of the selected spectral dips versus pump power, (c) experimental Q-factor as a function of the value of pump power, (d) the selected spectral dips versus pump power for MDA-WGM with different coating cycles and different MNPs concentrations.

The observed optical tuning effect in the proposed MDA-WGM resonator system can be explained by the light-to-heat conversion properties of MNPs, leading to a decrease of the effective RI of the LCs under the influence of the pump laser radiation. The corresponding temperature-induced wavelength shift can be determined using the following equation [23]:

$$\Delta\boldsymbol{\lambda} = \boldsymbol{\lambda}(\boldsymbol{\alpha}\Delta\boldsymbol{T} + \frac{\mathbf{1}}{\boldsymbol{n_{core}}}\frac{\boldsymbol{dn_{core}}}{\boldsymbol{dT}}\Delta\boldsymbol{T} + \frac{\mathbf{1}}{\boldsymbol{n_{wall}}}\frac{\boldsymbol{dn_{wall}}}{\boldsymbol{dT}}\Delta\boldsymbol{T}) \qquad (5)$$

where α is the thermal expansion coefficient of the cylindrical WGM resonator, $\frac{\boldsymbol{dn_{core}}}{\boldsymbol{dT}}$ and $\frac{\boldsymbol{dn_{wall}}}{\boldsymbol{dT}}$ are the thermo-optic coefficients of the nematic LCs and the silica capillary, $\boldsymbol{n_{core}}$ and $\boldsymbol{n_{wall}}$ are the effective RIs of the nematic LCs and silica capillary, respectively. ΔT is the temperature change of the LCs due to the heat dissipation by the MNPs. The thermal-expansion-induced wavelength shift for such a resonator can be neglected due to the small expansion coefficients of the silica (in the order of 10^{-6} K^{-1}[24]) and the limited volume of the nematic LCs inside the capillary. It should be noted that the thermo-optic response of the LC material dominates the induced wavelength shift, $\boldsymbol{\lambda}\frac{\mathbf{1}}{\boldsymbol{n_{core}}}\frac{\boldsymbol{dn_{core}}}{\boldsymbol{dT}}$ resulting in a blue shift with the increase of temperature since the thermo-optic coefficient of the silica capillary (~10^{-5} K^{-1}) is negligibly small[24,25]. This explanation is in a good agreement with the experimental data in Fig. 6(b).

To investigate the photothermal effect resulting from the BBS, the transmission spectra of the proposed WGM resonator system were analyzed at different power levels of the broadband light source while the pump laser was switched off. It should be noted that every data point was collected after the setup reached a stable state to reduce the errors. Fig. 7(a) shows the transmission spectra of the MDA-WGM with the half-taper with the highest sensitivity (3-coating cycles, 10 mg/ml MNPs concentration) collected at the BBS power levels of 3.06 mW, 5.34 mW, 7.74 mW, and 10 mW. As can be seen from the graph, the BBS power increase from 3.06 mW to 10 mW also resulted in a linear blue shift of the MDA-WGM spectra. Fig. 7(b) illustrates the dependence of the selected WGM dips (at circa 1545 nm) versus the BBS power. The resonance wavelength shift is approximately 4.1 nm as the power of the BBS increases, which demonstrates that the BBS also causes the photothermal effect and contributes the WGM wavelength shift. In order to ensure the accuracy of the results, the power of the BBS was fixed at 3.06 mW for all the MDA-WGM tuning experiments.

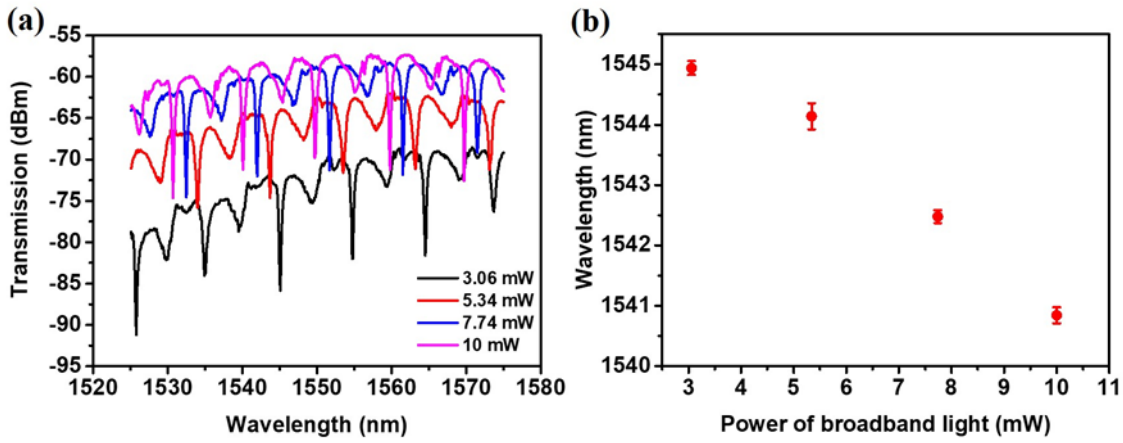

Fig. 7. (a) Transmission spectra of the MDA-WGM with a 3-coating cycles half-taper (10 mg/ml MNPs concentration) at different values of BBS power, (b) experimental data of the selected spectral dips versus BBS power.

Finally, thermo-optical tuning schemes using the photothermal effect of nanomaterials have been summarized in Table 1. Several materials with light-to-heat properties have been used to enhance the tuning performance of the WGMs with the help of the noncontact laser manipulation, such as Fe_3O_4[13], $NaNdF_4$[26], TiO_2[27], and xylene[28]. Due to the excellent photothermal effect of Fe_3O_4 and its broad absorption band, Fe_3O_4 MNPs have been widely used in photothermal effect based WGM tuning schemes under laser radiation at different wavelengths, as shown in literature[13–15,29–31]. Our result demonstrates the relatively high sensitivity compared with other photo-thermally induced WGM tuning schemes using Fe_3O_4 MNPs. Considering the high sensitivity of our proposed scheme, it is quite suitable for the next generation of tunable electronic and optical devices, such as filters, switches and lasers. In optical communication system, the wavelength selective characteristic of optical device is quite important, which enables us to select the desirable signals to be sent and make the communication more efficient. Due to the high sensitivity and ease of manipulation of our proposed scheme, transmission spectra can be selectively filtered or passed using an experimental setup by controlling the input laser power of 980 nm. In addition, the tunable laser with a small volume can be fabricated using dye-doped LCs infiltrated capillary, where the tuning performance can be realized by the photothermal effect of MNPs.

Tabel 1. Different thermo-optic tuning of WGM resonators

Microcavity	Heating materials	Sensitivity	Tuning range	Pump wavelength
Silica microsphere resonator[31]	Fe_3O_4 NPs	0.2 nm/mW	13 nm	1550 nm
Photonic crystal fiber resonator[15]	Fe_3O_4 NPs	0.034 nm/mW	3.6 nm	980 nm

Grapefruit microstructured fiber resonator[29]	Fe_3O_4 NPs	0.106 nm/mW	5.32 nm	1550 nm
Silica capillary resonator[13]	Fe_3O_4 NPs	0.15 nm/mW	3.3 nm	1527 nm
Silica capillary resonator[14]	Fe_3O_4 NPs	0.0382 nm/(mW·mm^{-2})	0.15 nm	532 nm
Silica microbottle resonator[30]	Fe_3O_4 NPs	22 pm/mW	0.68 nm	1550 nm
Nematic LCs infiltrated silica capillary resonator (this work)	Fe_3O_4 NPs	0.256 nm/mW	10.43 nm	980 nm
Hollow silica microsphere resonator[26]	$NaNdF_4$ NPs	2.95 nm/(W ·mm^{-2})	4.95 nm	793 nm
Polymer-coated microsphere resonator[32]	$NaNdF_4$ NPs	1.96 nm/(W ·mm^{-2})	2 nm	793 nm
TiO_2 coated microsphere resonator[27]	TiO_2 film	0.43 nm/mW	220 pm	980 nm
Polymer coated capillary resonator[28]	Polymer-doped xylene	0.58 nm·W^{-1} ·cm^{-2}	13 nm	940 nm

5. Conclusion

In conclusion, we investigated thermo-optic tuning of WGMs in a microcapillary resonator filled with nematic LCs theoretically and experimentally. Our theoretical analysis showed that a decrease in the thickness of the capillary resonator leads to an increase in the sensitivity of the WGM spectrum to the core material's RI and thus to temperature. From the experiments it is also found that increasing the thickness of the MNPs coating on the fiber taper surface by increasing the number of coating cycles leads to a stronger photo-thermal effect and to a larger change of the LC material's RI within the capillary core. Thermo-optic tuning of the WGM resonances with sensitivity to the pump power of 256.63±5.67 pm/mW and tuning range of 10.43 nm has been experimentally demonstrated. In this work, we proposed an enhanced WGM tuning scheme by increasing the coating thickness of the MNPs on the surface of the tapered fiber. Ideally, the tuning performance can be further increased by a stronger photothermal effect using a tapered fiber with a larger coating thickness. It should be noted the thickness of the coating cannot be limitlessly increased as the inserting process of the tapered fiber would be extremely difficult with the increase of the coating thickness. Furthermore, the heat transfer between MNPs and the LCs can be blocked by the multiple layers of MNPs because only the MNPs near the surface of the fiber-taper experience a strong photothermal effect. And there is a possibility that the WGM tuning scheme would be less effective if the temperature of the capillary exceeded the clearing point of LCs, resulting in a decrease of the Q factor of the WGMs resonator. Although the optimum layer thickness is difficult to determine due to the hard detection of the temperature inside of

the capillary, the proposed tuning scheme with enhanced sensitivity and larger tuning range still has many potential applications in future tunable optical filters and sensors.

CRediT authorship contribution statement

Zhe Wang designed, fabricated, studied the structure experimentally and drafted the manuscript. Arun Kumar Mallik contributed to numerical simulations and data analysis. Fangfang Wei: contributed to the design of experimental setup and fabrication. Zhuochen Wang and Anuradha Rout contributed to experiments and data analysis. Qiang Wu provided useful discussion and contributed to the analysis of the results. Yuliya Semenova supervised the project, co-wrote the manuscript and gave suggestions at all stages.

Declaration of Competing Interest The authors declare that they have no conflict of interest.

Data availability Data will be made available on reasonable request.

Acknowledgements This research was funded by the TU Dublin Fiosraigh Scholarship Award 2019.

References:

[1] V.S. Ilchenko, A.A. Savchenkov, A.B. Matsko, L. Maleki, Nonlinear Optics and Crystalline Whispering Gallery Mode Cavities, Phys. Rev. Lett. 92 (2004) 4. https://doi.org/10.1103/PhysRevLett.92.043903.

[2] H. Wang, R. Xu, J. Zhang, W. Zhou, D. Shen, Ultranarrow filter based on Fano resonance in a single cylindrical microresonator for single-longitudinal-mode fiber lasers, Opt. Express. 27 (2019) 22717. https://doi.org/10.1364/oe.27.022717.

[3] P. Wang, R. Madugani, H. Zhao, W. Yang, J.M. Ward, Y. Yang, G. Farrell, G. Brambilla, S. Nic Chormaic, Packaged Optical Add-Drop Filter Based on an Optical Microfiber Coupler and a Microsphere, IEEE Photonics Technol. Lett. 28 (2016) 2277–2280. https://doi.org/10.1109/LPT.2016.2591959.

[4] A. Taeb, M.A. Basha, S. Gigoyan, M. Marsden, S. Safavi-Naeini, Label-free DNA sensing using millimeter-wave silicon WGM resonator, Opt. Express. 21 (2013) 19467. https://doi.org/10.1364/oe.21.019467.

[5] M.S. Luchansky, R.C. Bailey, High-Q optical sensors for chemical and biological analysis, Anal. Chem. 84 (2012) 793–821. https://doi.org/10.1021/ac2029024.

[6] Y. Du, C.L. Zou, C. Zhang, K. Wang, C. Qiao, J. Yao, Y.S. Zhao, Tuneable red, green, and blue single-

mode lasing in heterogeneously coupled organic spherical microcavities, Light Sci. Appl. 9 (2020). https://doi.org/10.1038/s41377-020-00392-7.

[7] S. Lane, F. Marsiglio, Y. Zhi, A. Meldrum, Refractometric sensitivity and thermal stabilization of fluorescent core microcapillary sensors: theory and experiment, Appl. Opt. 54 (2015) 1331. https://doi.org/10.1364/ao.54.001331.

[8] X. Jin, Y. Dong, K. Wang, Stable controlling of electromagnetically induced transparency-like in a single quasi-cylindrical microresonator, Opt. Express. 24 (2016) 29773. https://doi.org/10.1364/oe.24.029773.

[9] G.N. Conti, S. Berneschi, A. Barucci, F. Cosi, S. Soria, C. Trono, Fiber ring laser for intracavity sensing using a whispering-gallery-mode resonator, Opt. Lett. 37 (2012) 2697. https://doi.org/10.1364/ol.37.002697.

[10] X. Liu, Q. Lu, L. Fu, X. Chen, X. Wu, S. Xie, Coupled-mode induced transparency via Ohmic heating in a single polydimethylsiloxane-coated microbubble resonator, Opt. Express. 28 (2020) 10705. https://doi.org/10.1364/oe.390593.

[11] J.T. Gohring, P.S. Dale, X. Fan, Detection of HER2 breast cancer biomarker using the opto-fluidic ring resonator biosensor, Sensors Actuators, B Chem. 146 (2010) 226–230. https://doi.org/10.1016/j.snb.2010.01.067.

[12] J.D. Suter, D.J. Howard, H. Shi, C.W. Caldwell, X. Fan, Label-free DNA methylation analysis using opto-fluidic ring resonators, 2009 Annu. Int. Conf. IEEE Eng. Med. Biol. Soc. (2009) 2760–2762. https://doi.org/10.1016/j.bios.2010.08.050.

[13] Y. Liu, L. Shi, X. Xu, P. Zhao, Z. Wang, S. Pu, X. Zhang, All-optical tuning of a magnetic-fluid-filled optofluidic ring resonator, Lab Chip. 14 (2014) 3004–3010. https://doi.org/10.1039/c4lc00236a.

[14] Y. Li, H. Zhang, B. Liu, J. Wu, B. Song, D. Yan, C. Yang, Tuning of whispering gallery modes in a magnetic-fluid-infiltrated silica capillary based on lateral pumping scheme, J. Opt. (United Kingdom). 19 (2017). https://doi.org/10.1088/2040-8986/19/1/015801.

[15] W. Lin, H. Zhang, B. Liu, B. Song, Y. Li, C. Yang, Y. Liu, Laser-tuned whispering gallery modes in a solid-core microstructured optical fibre integrated with magnetic fluids, Sci. Rep. 5 (2015) 1–10. https://doi.org/10.1038/srep17791.

[16] V. Kavungal, G. Farrell, Q. Wu, A.K. Mallik, Y. Semenova, Thermo-optic tuning of a packaged whispering gallery mode resonator filled with nematic liquid crystal, Opt. Express. 26 (2018) 8431. https://doi.org/10.1364/oe.26.008431.

[17] X. Zhu, Z. He, H. Zhu, W. Zhang, Spectrally programmable fiber microcavity laser with dye-doped liquid crystals, Opt. Laser Technol. 158 (2023) 108860. https://doi.org/10.1016/j.optlastec.2022.108860.

[18] R.C. Xie, S.Y. Tsay, J.J. Wu, C.C. Kuo, H. Zhang, J.H. Lin, Manipulation of plasmonic random laser from dye-doped liquid crystals inside photonic crystal fiber by the electric field, Opt. Laser Technol. 151 (2022) 108013. https://doi.org/10.1016/j.optlastec.2022.108013.

[19] Z. Wang, A.K. Mallik, F. Wei, Z. Wang, A. Rout, Q. Wu, Y. Semenova, Thermo-optic tuning of a

nematic liquid crystal-filled capillary whispering gallery mode resonator, Opt. Express. 29 (2021) 23569. https://doi.org/10.1364/oe.432103.

[20] F. Wei, A.K. Mallik, D. Liu, Q. Wu, G.Di. Peng, G. Farrell, Y. Semenova, Magnetic field sensor based on a combination of a microfiber coupler covered with magnetic fluid and a Sagnac loop, Sci. Rep. 7 (2017). https://doi.org/10.1038/s41598-017-05199-y.

[21] A. Meldrum, F. Marsiglio, Capillary-Type Microfluidic Sensors Based on Optical Whispering Gallery Mode Resonances, Rev. Nanosci. Nanotechnol. 3 (2014) 193–209. https://doi.org/10.1166/rnn.2014.1054.

[22] T.A. Kumar, M.A. Mohiddon, N. Dutta, N.K. Viswanathan, S. Dhara, Detection of phase transitions from the study of whispering gallery mode resonance in liquid crystal droplets, Appl. Phys. Lett. 106 (2015). https://doi.org/10.1063/1.4906615.

[23] J.D. Suter, I.M. White, H. Zhu, X. Fan, Thermal characterization of liquid core optical ring resonators, IEEE/LEOS Int. Conf. Opt. MEMS Their Appl. Conf. 2006. 46 (2006) 177–178. https://doi.org/10.1109/omems.2006.1708323.

[24] G. Ghosh, Temperature Dispersion of Refractive Indexes in Some Silicate Fiber Glasses, IEEE Photonics Technol. Lett. 6 (1994) 431–433. https://doi.org/10.1109/68.275509.

[25] S. Mathews, G. Farrell, Y. Semenova, Liquid crystal infiltrated photonic crystal fibers for electric field intensity measurements, Appl. Opt. 50 (2011) 2628–2635. https://doi.org/10.1364/AO.50.002628.

[26] H. Li, X. Hao, Y. Li, L. Xu, B. Shi, L. Liu, Nanoheater-tuned whispering gallery mode lasing in liquid-filled hollow microcavities, Opt. Lett. 45 (2020) 815. https://doi.org/10.1364/ol.383024.

[27] H. Wan, Y. Lu, Z. Liang, Z. Shen, P. Gu, T. Hu, J. Chen, Tunable, single-wavelength fiber laser based on hybrid microcavity functionalized by atomic layer deposition, J. Light. Technol. (2022) 4–7. https://doi.org/10.1109/JLT.2022.3233138.

[28] B. Niu, X. Shi, K. Ge, J. Ruan, Z. Xu, S. Zhang, D. Guo, T. Zhai, An all-optical tunable polymer WGM laser pumped by a laser diode, Nanoscale Adv. 4 (2022) 2153–2158. https://doi.org/10.1039/d2na00025c.

[29] M. Deng, Y. Wang, L. Liu, M. Qin, Broadband laser-tuned whispering gallery mode in a micro-structured fiber embedded with iron oxide nanoparticles, Appl. Opt. 57 (2018) 4563. https://doi.org/10.1364/ao.57.004563.

[30] S. Zhu, L. Shi, S. Yuan, X. Xu, X. Zhang, All-optical control of ultrahigh-Q silica microcavities with iron oxide nanoparticles, Opt. Lett. 42 (2017) 5133. https://doi.org/10.1364/ol.42.005133.

[31] P. Zhao, L. Shi, Y. Liu, Z. Wang, S. Pu, X. Zhang, Iron-oxide nanoparticles embedded silica microsphere resonator exhibiting broadband all-optical wavelength tunability, Opt. Lett. 39 (2014) 3845. https://doi.org/10.1364/ol.39.003845.

[32] H. Li, X. Hao, Y. Li, R. Duan, T. Zhang, J. Li, Y. Yuan, L. Liu, Photothermal control of whispering gallery mode lasing in polymer-coated silica microcavity using high-efficiency nanoheater, J. Mater. Sci. 56 (2021) 570–580. https://doi.org/10.1007/s10853-020-05272-4.